International Journal of Innovative Technology and Interdisciplinary Sciences
www.IJITIS.org
ISSN:2613-7305
Volume 4, Issue 1, pp. 634-662, 2021
DOI: https://doi.org/10.15157/IJITIS.2021.4.1.634-662
Received February 15, 2021; Accepted March 22, 2021

Geotechnical Characterization and Rockfall Simulation Using Remote Mapping. A case of Carnsew Quarry in Penryn, Cornwall (UK)

Abdul Samson*, Jabulani Matsimbe, Steve Ghambi
Department of Mining Engineering, University of Malawi, Malawi
asamson@poly.ac.mw

ABSTRACT

Remote mapping involves obtaining rock slope data using laser scanning. The data is a collection of 3-D coordinates and typically includes intensity and colour information about objects present in the 3-D scene. Several software analyses were undertaken ranging from Split FX to stereographic projection to make sense of the data obtained by the method. Remote mapping has proved to be a very important and effective tool in terms of obtaining geotechnical data for observation and analysis. The rock slope section under consideration (Carnsew quarry) is an example of the need for remote mapping since hand mapping could not be achieved on the slope because of the safety hazard due to the steepness of the slope. Analysis of the slope data by kinematic analysis in Dips (stereographic projection) reveals a serious risk of failure that could result from either wedge or flexural toppling or both failure mechanisms. It is from these failure mechanisms that rockfall could originate from (through rocfall software analysis). This is true because of the steepness of the slope specifically the section above the haul road. The risk of rockfall possess a severe hazard on safety of workforce on the quarry mine. The height and energy possessed by rocks falling could also damage equipment on the mine. It was therefore, recommended that operations on this section of the slope be suspended for further geotechnical analysis to be done. Specifically, a cost benefit analysis was suggested to compare the cost of maintaining or stabilising the slope (control of wedge or flexural failure and rockfall) against the value of the slope section in terms of productivity.

Keywords: Slope characterisation, slope failure, remote mapping, slope stability, rockfall.

1. INTRODUCTION

Rockfall is one of the major problems faced by quarries, surface mining pits as well as road cuts across the world. The damage caused by rockfall can be very severe ranging from loss of property to loss of life. Over the years, a lot of research has been done to understand the science behind rockfall. The main focus has been characterisation of rock slopes and ascertaining the occurrence of rockfalls. However, further research has been done on the causes, the mechanics, and methods of analysis for rockfalls just to mention a few. The major concern behind all this research and interest in rockfall has been to make sure rock slopes (road cuts, mine slopes) are operational safe due to their destructive consequences. Problems associated with rock fall arise all over the world. Severe effects of rockfall usually occur in road cuts, cliffs near beaches and other rock slopes that are close to human interaction.

Over the years, analysis of rockfalls from data collection to the actual data analysis has undergone several changes and modifications. These modifications and changes have made rock slope characterisation and rockfall analysis in particular highly simplified and easy to conduct. Collection of geotechnical data for analysis has also changed from on-site data collection to remote mapping using state of the art equipment.

The main objective of this research was to conduct geotechnical characterisation, rockfall simulation and control on a rock slope using remote mapping. Specifically, the research looked at;

a) Geotechnical characterization using remote mapping;
b) Assessing the possibility of rockfall based on the geotechnical data obtained;
c) Assessing the possibility of failure mechanisms based on the geotechnical data; and
d) Rockfall simulation and control using 2-D rockfall software.

2. MATERIALS AND METHODOLOGY

2.1 Carnsew Quarry

Operated by transport infrastructure group Colas UK, Carnsew quarry has been a major producer of crushed Carnmenellis granite aggregate, supplying west and central Cornwall, with much of the production being coated for road construction. The quarry also supplies decorative silver granite aggregate, rock armour for sea defences and gabion stone for embankments and river protection [1].

The quarry is located in south west of England in the United Kingdom. The site in Penryn is close to the urban markets of Truro and Redruth and is about five kilometres north of Falmouth. Some of its production is transported by sea from Falmouth docks. Since its inception in the late 1940s, the quarry has had several consents and extensions. The major extensions were done in the 1980s.

A decision by Cornwall strategic planning committee late 2016 granted the quarry a new 80-year quarrying permission [1]. The permit will last until December 2095. The decision removes historic depth limitations, paving the way to extract very high-quality granite which was previously out of reach. The quarry mine will therefore be able to extract 22 million tonnes of granite until the permit expires.

Figure 1. Aerial view of Carnsew Quarry in Penryn, Cornwall. Source: Google earth [1]

2.2 Methods of data collection and mapping

The two major methods of data capture for geotechnical analysis are remote and hand mapping. Hand mapping is the first and ordinary method that has been used for data collection for so many years. Due to safety reasons and difficulty in reaching certain parts of a slope to get data, another way of obtaining data was introduced, hence the use of remote sensing. This method means obtaining data remotely for geological mapping and geotechnical analysis. Under remote sensing, there are two main methods that are used to capture data and these are photogrammetry and laser scanning. The Table 1 summarises the general comparison between remote and hand mapping.

Table 1. Methods of Mapping and their advantages and disadvantages [2].

Method of Mapping	Advantages	Disadvantages
Hand mapping	Certain features of the rock (e.g. persistence, roughness, etc.) require human judgement and can best be analysed by the human eye on site.	Possesses a great risk in terms of safety especially in high-rise and rocky slopes. Limited by difficulty in access to certain parts of a slope during data collection. Slow and tedious method. Fatigue can affect quality of data collected.
Remote Mapping	Ability to capture data over a wide range and the whole rock face at once. Ability to map inaccessible areas of a slope. Uniformity in data collection by eliminating human bias. Fastest method of collecting and analysing geotechnical data.	Requires a combination of both point cloud and photogrammetry data to make a comprehensive analysis. Requires familiarity with the systems used (from equipment set up to interpreting data acquired), hence may require extra training to understand the whole process.

2.2.1 Photogrammetry

Photogrammetry is described as the science of obtaining reliable information from physical objects through processes of recording, measuring, and interpreting photographic images [3-5]. Introduction of cheap and affordable devices (digital cameras, mobile phones, etc.) for capturing images has seen the images being processed using computers. Digital photographs are combined with surveying techniques to produce 3-D images that are easily visualised and manipulated on computer screens [3].

2.2.2 Laser Scanning

Whilst photogrammetry has been used for so many years, laser scanning is a new technique and has just been introduced for geological and geotechnical data collection recently. Laser scanning was first developed from single beam laser range finders, which were attached to surveying theodolites. They were able to pinpoint the position of a reflector station situated over the point of interest. In [6] it has been used this technology for geotechnical applications. They used non-reflector total stations to find fracture orientations of planes on a rock face.

Laser scanning uses one or more infrared lasers to collect spatial data from a scanned area. Two types of laser scanning are currently employed across the world, Time-Of-Flight (TOF) and Phase Shift. The basic principle behind TOF and phase shift is that the position of a point in 3D space can be calculated by measuring its distance and orientation from a known point using reflected laser pulses. The data used in this research was obtained using laser scanning which produced a point cloud image for geotechnical analysis.

2.3 Data source

Carnsew quarry is located in Penryn, Cornwall, UK. In April 2013, Colas UK, the owners of the quarry, requested Camborne School of Mines at University of Exeter to conduct a geotechnical analysis on one of the quarry walls due to the steep slope created during mining of the section. The quarry side possessed a danger of failure and could have resulted in a danger to the site workers mainly because at the toe of the slope was a haulage road. The main dangers associated with the slope were rock fall, due to the steep slope, and other failure mechanisms such as wedge, plane, and toppling depending on the rock discontinuity orientation and location on the slope.

The section of the site on which geotechnical analysis and rockfall simulation was done is located on the south-eastern part of the quarry site. Unfortunately, access to collect still pictures of the site and more especially the wall under analysis was not possible due to safety reasons. However, the aerial image below taken from google earth shows the section of the quarry slope on which point cloud data was obtained for geotechnical analysis.

Figure 2. Section of Carnsew quarry slope on which point cloud data [1].

Data was collected using a 3D laser scanning equipment. This device is used to collect three-dimensional geometric data. The data is a collection of 3D coordinates and typically includes intensity or colour information about objects present in the 3D scene. The data set is referred to as a point cloud and can be stored in a number of ways.

A combination of analyses was done on the data. This was done through importation of the data from one computer model to another. The point cloud data was analysed by Split FX. From Split FX the data was exported to stereographic projection modelling and Rockfall modelling software. On each computer modeller, an independent data analysis was done based on the capabilities of the modeller. The basic steps involved in designing and analysing the models were as follows: defining materials, defining sections and model creation [7]. Results of each analysis were combined to determine the potential for rockfall and other failure mechanisms.

2.4 Split FX

This is a commercial software/computer modeller compiled by Split Engineering. It interprets data obtained by laser scanning. There are several ways in which data can be interpreted on this computer model, but the mostly used section is converting the data from the point cloud image to stereographic projection. During data collection by scanning, the orientation of the slope is either automatically loaded by the scanning machine or fed into the point cloud data before analysis. Since the orientation of the slope is incorporated into the point cloud, determination of discontinuities becomes easy and straightforward.

The major use of Split FX is to obtain jointing data from the point cloud data and convert it into stereographic projection. Mapping of the slope on the point cloud data can be done either manually or automatically. Under automatic mapping, the software maps all the approximate joints, shears as well as cleverages. However, the amount of jointing mapped automatically depends on how good the point cloud data is. Normally, automatic mapping tends to leave a lot of data unmapped and this might be a step back when it comes to data analysis and drawing conclusions.

The best way to map point cloud data in the Split FX software is manually. Apart from being able to obtain comprehensive data, which could easily be left by automatic mapping, manual mapping allows one to rotate and view the slope in various angles. This allows one to map a lot of data from the point cloud. Rotating and viewing the data in different angles also allows the modeller to view certain joints, which could not be seen in another angle of view. There are several ways of manually obtaining jointing data from the point cloud. However, the two mostly used methods are either by patching or tracing. The method to use depends on which orientation is the joint clearly visible and the direction in which the scanning machine was during mapping.

Patching defines plane, which represents a discontinuity surface. This works better when the jointing is able to be seen perpendicular to the scanning machine. Patches are drawn on these visible portions. How big the patch drawn depends on the size of the patch being seen by the modeller.

A Trace is a two-dimensional lineation of a three-dimensional discontinuity surface that appears in a 2D image. Tracing works in the opposite way to patching. This maps joints which are easily seen and were taken directly parallel to the scanning machine. The stretch of the trace depends on the length of the section being traced.

Either using patching or tracing does not affect the stereographic data plotted on the other window of the software. This gives a first impression of the data as plotting is done. The more the data is mapped from the point cloud, the more comprehensive the data will

be in the stereographic projection. In turn, a more elaborate analysis can be made and a representative conclusion drawn from the analysis of the results. The stereo-net plotted is able to display data as either great circles or poles. However, poles project a clear picture than great circles as more and more data is plotted.

Furthermore, contouring can also be done on the plotted stereo-net to determine the concentration of poles. It is also possible to determine major sets of discontinuities based on the contours created. The Figures 10 and 11 have been illustrated in the appendixes to show point cloud data, patching and tracing done on the point cloud data.

2.5 Stereographic Projection (Dips)

Discontinuity data was exported from Split FX to Dips software for further analysis. This was done to determine failure mechanisms on the slope such as plane, wedge as well as toppling. A more comprehensive analysis requires kinematic analysis to determine actual failure mechanisms based on slope characteristics. This include, slope angle, slope friction angle as well as the rock strength. However, in this research, stereographic projection was used basically to determine probable failure mechanisms with the help of the slope angle. As mentioned above, access to the site to obtain further data was not possible. Nevertheless, based on other research, average strength of granite alongside its theoretical friction angle was used in kinematic analysis in order to give a representative picture of the analysis.

The friction angle of carnmenellis granite ranges from 28.5 to 32.5 degrees [8]. This was the range of friction that was used during kinematic analysis of the data. Furthermore, the average strength of carnmenellis granite is 103MPa and increases at a rate of 30MPa/km with depth [9]. The rock type at Carnsew quarry is the same as that one described in the paper written by Pine and others. The mines also fall in the same location of UK.

2.5.1 Kinematic Analysis

Point cloud data on the poles plotted either by patches or traces was exported into an excel sheet and fed into dips software for stereographic projection analysis. The data consisted dip and dip direction of the discontinuities. From the design of model set, a bank of filters runs in parallel at every time, each based on a particular model, to obtain the model-conditional estimates. The overall state estimate is a probabilistically weighted sum of these model-conditional estimates [10]. A combination of traces and patches totalled 790 poles, which were plotted on the stereo-net in Dips software. Based on the cross-sections obtained from the point cloud data for rockfall analysis, both the height and angle of the slope was obtained.

Other parameters such as dip direction and friction angle were kept constant, as they could not vary as the slope angle (dip) did. The dip direction was approximated to be around 300° (northwest direction) as the mean value since the slope section was not dipping perfectly in a definite direction. The below Table 2 shows slope parameters used to conduct kinematic analysis on the slope.

Table 2. Slope parameters used in kinematic analysis

	Dip (°)	**Dip Direction (°)**	**Friction angle (°)**	**Lateral limits (°)**
Minimum Slope angle	**45**	**300**	**30**	**20**
Mean Slope angle	**65**	**300**	**30**	**20**
Maximum Slope angle	**85**	**300**	**30**	**20**

The slope angle (dip) was varied to determine the effect of variation of the angle on the geotechnical failure mechanisms. Furthermore, this was done to determine the extent of failure modes as a result of varying the slope angle. In addition, some sections of the slope were steeper than other sections, hence the variation to make a realistic representation of the slope. Failure extent was determined by categorising critical failure percentage as obtained from the kinematic analysis into three categories: ***minimal***, ***moderate*** and ***critical failure***.

A further analysis was done on the slope to determine the sensitivity of the failure mechanisms to variation of slope parameters. These were friction angle, slope angle, the overall slope dip direction as well as lateral limits of kinematic analysis. A range of values was selected together with the mean values for sensitivity analysis. The values are given in the Table 3.

Table 3. Parameters used for sensitivity analysis in kinematic analysis

Parameter	**Minimum Value**	**Mean Value**	**Maximum Value**
Slope Dip	45°	65°	85°
Slope Dip direction	280°	300°	320°
Friction angle	28°	30°	32°
Lateral Limits	10°	20°	30°

2.6 Rockfall simulation (Rocfall)

Further analysis was done to determine the possibility of rockfall using rockfall software by rocscience. Three cross sections from the point cloud data were obtained using AutoCAD software. The three sections included one on both far ends of the slope and another one on the centre section of the slope. They were then exported to rocfall software for analysis. This was done to observe the variation of rockfall in terms of the section of the slope. Default parameters based in the rockfall software in terms of normal, tangential restitution and dynamic and rolling friction were used since no such data was obtained on the actual slope and to make sure the results obtained were conservative. Table 4 illustrate parameters used for rockfall simulation.

Table 4. Default slope parameters used for rockfall simulation

	Mean	Distribution	Standard Deviation	Relative Minimum	Relative Maximum
Normal restitution	0.35	Normal	0.04	0.12	0.12
Tangential restitution	0.85	Normal	0.04	0.12	0.12
Dynamic friction	0.5	Normal	0.04	0.12	0.12
Rolling friction	0.15	Normal	0.02	0.06	0.06

As explained above, only deterministic analysis was done. The slope was divided into three sections. The slope was divided into ***left section***, the ***centre section*** and ***right section*****.** In the Table 5 are shown the cross-section parameters of the slope sections under consideration. The dimensions/measurements were obtained from the imported files in AutoCAD software.

Table 5. Dimension of the slope sections used for rockfall simulation

Slope section	Slope height (m)	Horizontal length (m)
Right section	95	56
Middle section	89	77
Left section	78	86

The rock type used was granite and has the density of 28 kN/m^3. It should also be noted that during simulation, the patched section (yellowish, Figure 7) of the slope represents the section where the haulage road was located on the slope.

During rockfall simulation, the different sections of the slope were seeded with rocks at three sections; the top most part of the slope, at the middle just above the haulage road, and the last section slightly above the bottom of the slope. This was done to determine the effect of the falling rocks from various heights on the slope. The main section of major interest was the road section. Normally this is the section that would be used by staff and equipment hence poses the highest risk in terms rockfall.

The first analysis was to simulate the fall of a single rock seeded at the designated three sections mentioned above on each slope section (far right, centre and far left) and observe the behaviour of the rock as it falls down the slope with much observation focused on the road section. Furthermore, the slope sections were also seeded with 50 rocks on each section of the slope. Again, the focus was on the haulage road section of the slope. Figure 5 was chosen to make sure the simulation was conservative (worst-case scenario).

In addition, observation was also made on the kinetic energy of the rocks as they fell through the slope. Graphs of the number of rocks falling and their kinetic energy were plotted for each section of the slope specifically on the road section. This was done to

determine the destructive force the rocks carried as they fell down the slope on to the road section and the number rocks carrying that destructive energy.

3. EXPERIMENTAL RESULTS

The results were divided into two categories, geotechnical assessment (discontinuity related) including characterisation and rockfall simulation/analysis.

3.1 Geotechnical Characterization

3.1.1 Stereographic projection

The Figure 3 shows results of stereographic projection in dips software. Table 6 shows major sets identified using clustering during stereographic projection analysis in Dips software. Three major sets were observed with other random poles on the stereo-net.

Table 6. Major sets identified by clustering.

Set ID	Dip (°)	Dip Direction (°)
1m	82	249
2m	75	344
3m	45	104

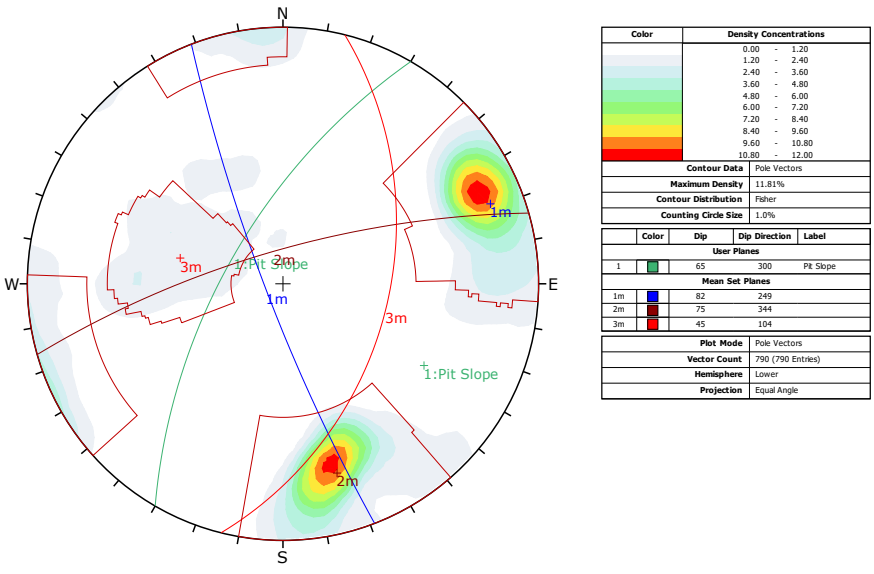

Figure 3. Major sets and planes with average pit slope

3.1.2 Failure mechanisms

Table 7 illustrate results of the geotechnical analysis conducted on the slope to determine slope stability and possible failure mechanisms based on the slope angle (dip). These are the results of the kinematic analysis.

Table 7. Results of geotechnical analysis undertaken on the slope using kinematic analysis

Failure Mechanism	Plane Sliding	Wedge Sliding	Direct Toppling	Flexural Toppling	Comment
Slope Angle	**Minimum Slope angle (45°)**				
Minimal failure	✓	✓	✓	✓	Critical percentage failure less than 10%
Moderate failure					
Critical failure					
Slope Angle	**Mean Slope angle (65°)**				
Minimal failure	✓		✓		Critical percentage failure less than 10%
Moderate failure		✓		✓	Critical percentage greater than 10% but less than 30%
Critical failure					
Slope Angle	**Maximum Slope angle (85°)**				
Minimal failure	✓		✓		
Moderate failure					
Critical failure		✓		✓	Critical percentage failure greater than 30%

3.1.3 Sensitivity analysis on failure mechanisms

The results of sensitivity analysis done on the slope to determine the effect of varying slope parameters (slope dip, friction angle, etc.) on the criticality of failure for each failure mechanism analysed were plotted graphically. Figures 4 until 6 represents sensitivity analysis for all the failure mechanisms under consideration.

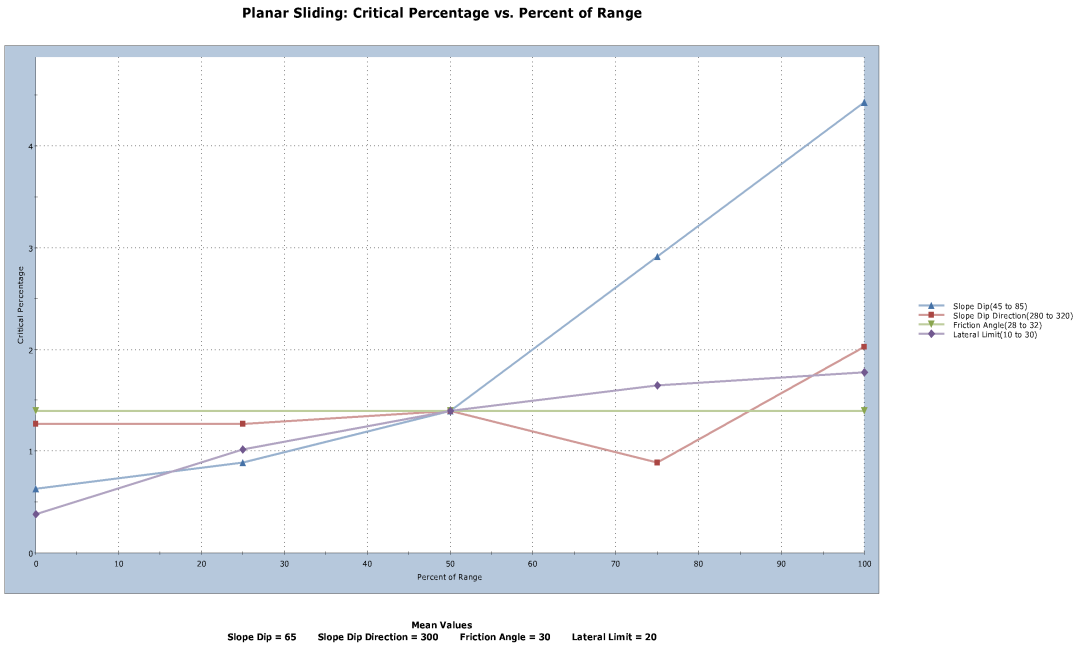

Figure 4. Sensitivity analysis on planar failure

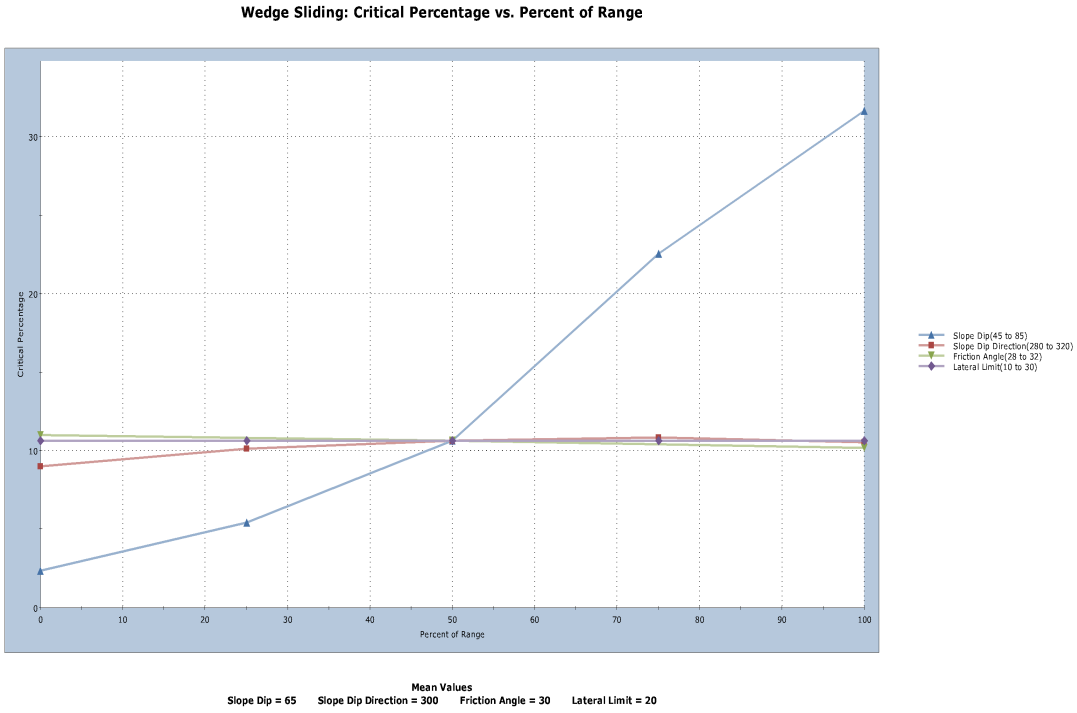

Figure 5. Sensitivity analysis on Wedge Sliding

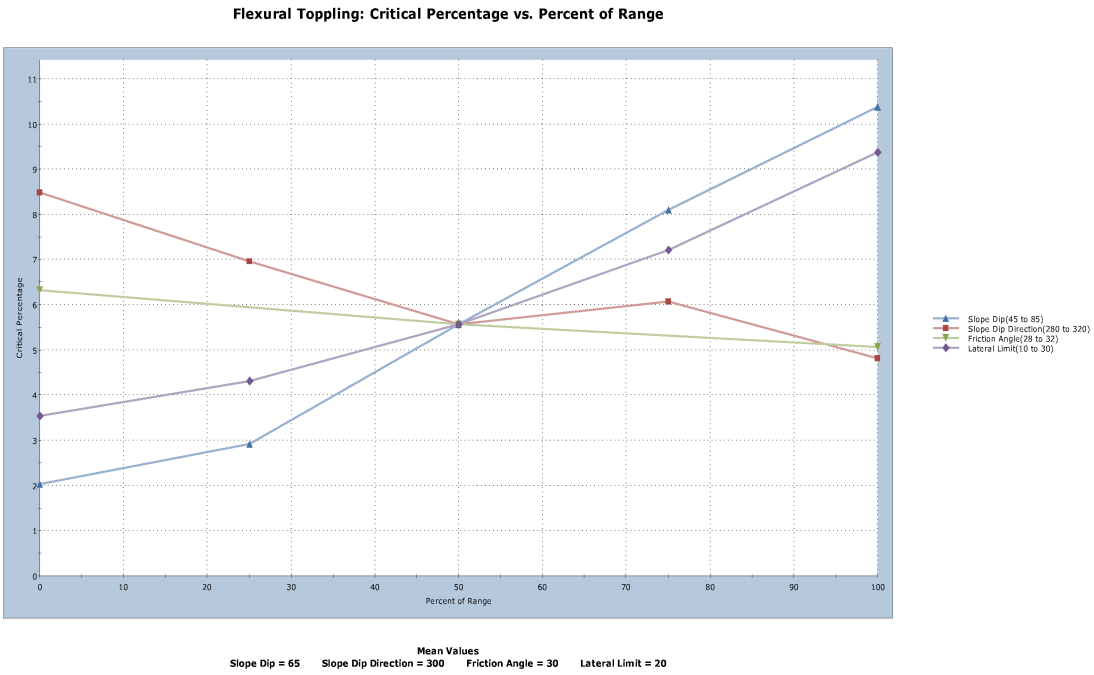

Figure 6. Sensitivity analysis on flexural toppling

3.2 Rockfall Simulation

Figures 7 until 9 illustrated shows simulation results of rockfall conducted in rockfall software.

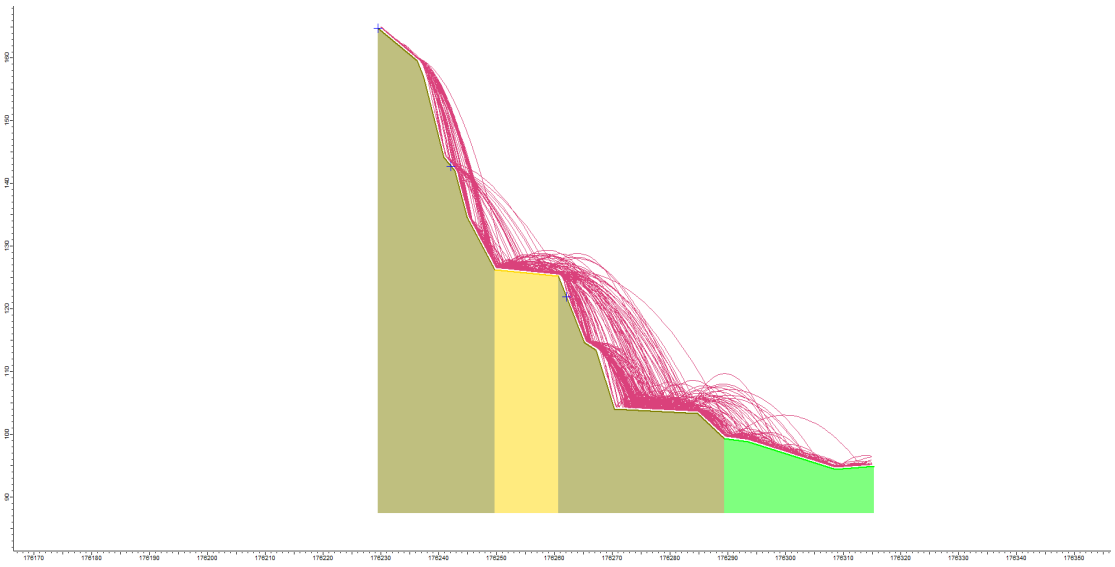

Figure 7. Left cross-section of the slope with 50 seeded rock at each section.

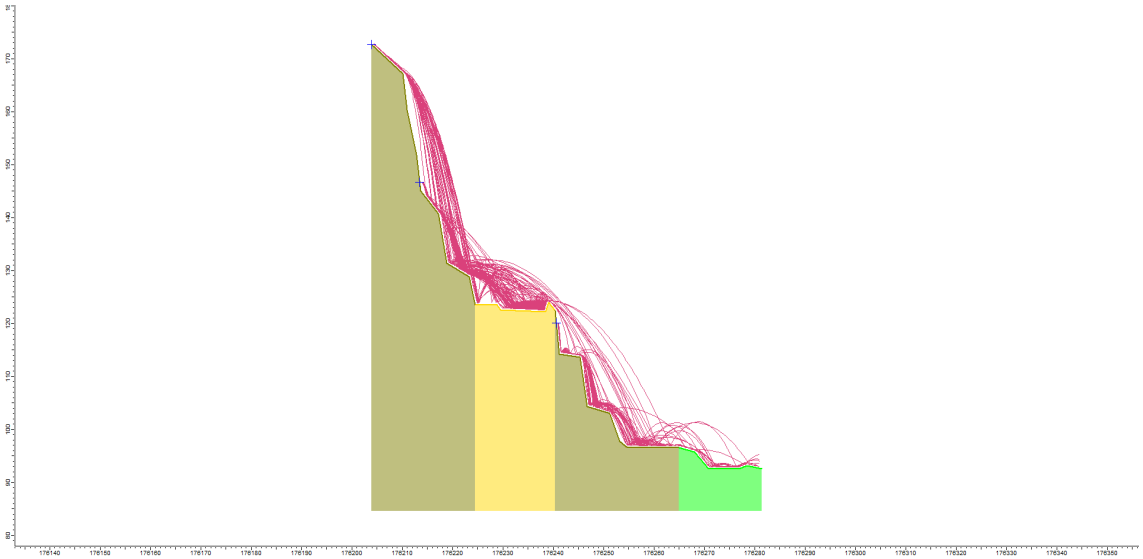

Figure 8. Middle/centre cross-section of the slope with 50 seeded rock at each section.

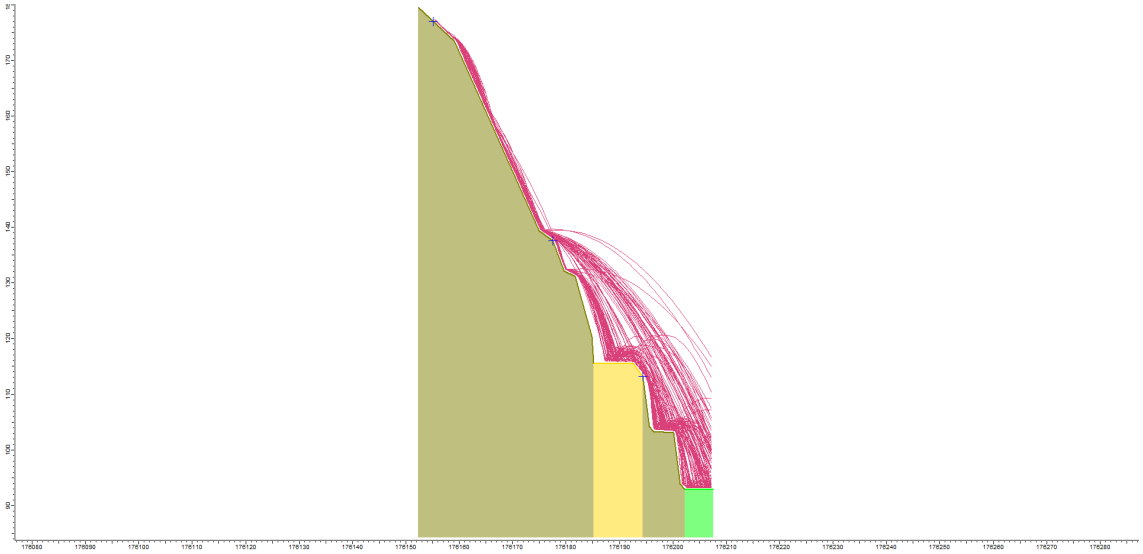

Figure 9. Right cross-section of the slope with 50 seeded rock at each section.

4. SIMULATION RESULTS

The analysis of the results (geotechnical characterisation and rockfall simulation) was discussed separately. This was done to make a comprehensive overview of the results obtained on the two slope characterisation analyses.

4.1 Geotechnical Analysis

The main emphasis is placed on the discontinuity related failure analysis. Stereographic projection (Dips) software produced three major sets as seen in the results. One may argue that only two sets (1m and 2m) were more pronounced and clearly visible than set 3m. Sometimes the set up and location of the laser-scanning equipment may miss certain data portions of the slope. The third set (nearly horizontal) came in because of two main reasons:

Firstly, the rock type under investigation is granite. Regardless of lack of site visit to see the actual slope, intact granite possesses an orthogonal type of jointing with one of the discontinuity surfaces nearly horizontal. Furthermore, the rock type surrounding the area (for example rock type at CSM test mine) is also orthogonal/cuboid. Since the sites are close to each other, it was deduced that the rock at Carnsew quarry should possess the same characteristics. An orthogonal type of jointing occurs mainly in high strength and intact rocks. This is characterised by having three major jointing surfaces that eventually form sugar like cubes within the rock with one of the joints being nearly horizontal.

Secondly, Dips software indicates that for a cluster to become a set it has to have a concentration of poles of more than 6% of the total around a section of the stereo-net. However, even though this was not achieved on this set (3m); the number of poles concentrated around this nearly horizontal set was more than 100. The fact that a large number of poles were clustered, though not specifically concentrated, around that centre section of the stereo-net was enough to make this cluster a set.

As seen from the dips results, the three sets constitute an orthogonal type of jointing typical for a granite intact rock with one of the sets approximately horizontal.

Under geotechnical characterisation, the main focus will be on the failure mechanisms observed during data analysis. Regardless of the fact that certain failure mechanisms were not very pronounced as compared to the others, their presence (observation) is enough to be given a closer attention. Again, through stereographic analysis, it is not known where exactly and when a failure could occur, and again the magnitude of that failure type, a thorough discussion of all the failure mechanisms observed becomes necessary.

4.1.1 Plane failure

Due to the dipping direction of the slope, it is observed that no set of discontinuity is directly susceptible to plane failure. Applying the conditions used to ascertain planar failure and considering the mean slope angle, out of the four critical conditions only one applies here. The friction angle (30°) is less than the angles of all the discontinuity sets observed. Looking at the other conditions, the slope angle is less than the dip angle of the two sets (1m and 2m), hence creating a condition not possible for daylighting to occur. Set 3m has a dip angle lower than the slope mean angle, however, this discontinuity set dips into the slope. Furthermore, it is observed that all the discontinuity sets have dip directions that do not fall within ±20° of the dip direction for the slope in order to daylight on the slope.

In addition, looking at the results given in Table 7 in the results section it is noted that varying the slope angle does not affect the results. From the results, minimal change is observed as the slope angle is varied from 45° to 85° as seen by the low percentage in criticality for failure (see Figure 12 to 14 in appendixes). The failure envelope does not capture the areas of high concentration of poles to necessitate critical failure. An increase in the slope angle therefore does not have any further effect on failure rather than widening the envelope in which a few more poles are captured that would result in planar failure.

An independent sensitivity analysis on the overall mean slope angle (65°) as given in Figure 4 for the slope parameters reveals that the slope planar failure has selective sensitiveness to some of the slope parameters. As noted from the chart, increasing the slope angle of the slope results in an increase in the critical percentage failure due to planar. This has been attributed to the fact that the increase of the slope angle widens the failure envelope hence capturing several poles. The same scenario is observed with the lateral limits.

A nearly constant behaviour is observed when friction is varied. As seen from the sensitivity chart varying the friction angle has no effect on the slope failing in planar. A better explanation for this would be that friction angle creates the margin of the failure envelope, and looking at the results in the stereographic projection shows that the margins created by friction do not capture any significant poles to create a noticeable critical failure.

Increasing the slope dip direction from the minimum value to the mean results in no significant change in failure. It however increases after the mean value and the rate of change further increases as the angle approaches 310°. This happens because as the slope dip direction increases above 310° the failure envelope starts to engulf set 2m. This results in increasing the percentage of poles that are covered by the failure envelope as the concentration of poles increases within set 2m.

From the results, only set 1m and 2m can undergo planar failure but not set 3m. Set 3m dips into the slope and this creates a condition not possible for planar failure to take place.

4.1.2 Wedge failure

Set 1m and 2m deep steeply out of the slope creating two nearly vertical joints and forming a wedge like structure. Since the two sets are steep, the plane of intersection is very steep as well dipping at approximately above 70°. Set 3m acts as a releasing structure of the wedge since it dips nearly horizontal cutting across the two sets creating a wedge above.

The main controlling factor for a wedge to form is the intersection plane. This works in the same way as plane failure. For wedge failure to take place, the intersection plane (dip) angle must not exceed the slope angle dip. This explains why there is minimal or no significant wedge failure for 45° and 65° slope angles (see Table 7 and Figures 15 to 17 in appendixes). The second condition is that the intersection plane must daylight on the slope plane. However, this usually goes together with the first condition. Daylighting only happens when the slope angle is greater than the dip angle of the discontinuity set. As such, slope angles of 45° and the mean slope (65°) still do not entirely satisfy this condition. Regardless of the set of discontinuity angle being greater than the slope angle, it should be noted that some of the poles in the set could be below the angle of the slope. This explains the low percentages observed with slope angles 45° and 65°.

The third condition is met by all the discontinuity sets. All the sets dip at angles greater than the friction angle (30°) hence potential for wedge failure. Other wedges are formed by sets 1m and 3m as well as sets 2m and 3m. However, these do not pose any threat to the slope because they both have intersection planes that dip into the slope.

Slope angle of 85° has the highest threat and risk of wedge failure. This is mostly attributed to the fact that this slope angle satisfies all the conditions necessary for a wedge to form, to daylight and be able to slide out of the slope. The slope angle is greater than the dip angle of the intersection plane (70°). This automatically makes the intersection plane to daylight out of the slope. As seen from the results, a high risk of wedge failure (31%) is observed at this slope angle.

Sensitivity analysis conducted on wedge failure indicates a low sensitiveness of the failure due to varying of the slope parameters. From the chart in figure 5, it is observed that failure due to wedge is highly sensitive to the slope angle. There are steady jumps of increase in the critical percentage as the slope angle is increased with the highest critical percentage observed at the maximum angle (85°). This tallies with the observation already made above and the same explanation can be applied here. The rest of the

parameters do not have significant effect on the slope failure as they are varied. Varying dip direction angle, friction angle and lateral limits within the given limits still ends up creating a failure envelope within the same region, which creates a failure envelope governed by the slope angle.

Therefore, a high risk of wedge failure should be expected as the slope angle increases. Considering the site of our interest, this applies to the upper section of the slope where the slope angle is significantly steep (above 85°).

4.1.3 Direct Toppling

Direct toppling is achieved through several ways. From the results obtained it is observed that both basal and oblique toppling occurs. A constant critical percentage risk (6.6%) for oblique toppling is observed throughout the different slope angles (45°, 65°, and 85°) used. The friction cone used controls oblique toppling which is also referred to as secondary toppling. Since friction angle is kept constant, oblique toppling follows this friction envelope and remains within the confinement of this envelope regardless of a change in the slope angles used. Furthermore, oblique toppling is not controlled by assigned slope lateral limits; hence, the failure envelope covers the entire view (180°) section of the slope in the given direction as observed in the stereo-net kinematic analysis (given by yellow failure envelope in the stereo-net) in the appendixes at Figures 21 and 22.

Primary toppling (direct toppling) involves basal planes and critical intersections. This is the critical type of toppling failure and occurs within the lateral limits of the dip direction (given by red envelope on the stereo-net). No set of discontinuity is directly linked to this failure in the results. However, increasing the slope angle increases the failure envelope. As such, a small increase is noted in the critical failure percentage as the slope angle is varied from 45° to 85°. This happens because the number of poles engulfed by direct toppling failure envelope increases as the slope angle together with the failure envelope increases as well.

The basic principle for direct toppling involves two sets of discontinuities with one slightly dipping into the slope and the other creating a base plane for rotation or tipping. A low critical percentage for direct toppling is observed with all the slope angles used. Furthermore, for toppling to occur, rectangular and nearly vertical blocks of rocks need to form. Referring to the dip angles of the discontinuity sets, these blocks can only form when the slope angle reaches 70° and beyond. With this in mind, one would therefore expect the rock blocks to form at a slope angle of 85°. This does not happen (as given by the low percentage failure) because the failure envelope does not fall within the two major sets of discontinuities (set 1m and 2m). However, another condition that would necessitate direct toppling is the fact that the dip of the two major discontinuities is greater than the friction angle. This explains the low percentage of failure recorded in relation to the slope angles.

A composite sensitivity analysis on direct toppling for the parameters could not be possible since this failure mechanism is composed of several sub-failure mechanisms. From the sensitivity analysis, it is observed that direct toppling is not affected by the friction angle. There is no change in direct toppling as the friction is varied. There is no sliding of blocks in direct toppling; rather the created rectangular blocks fail by means of tilting and rotation out of the slope face. However, there is a slight and/or minimal change recorded in oblique critical failure percentage as the friction angle is varied. The

magnitude of friction angle controls the extent of oblique failure as alluded in the subsequent paragraphs.

Like in friction sensitivity, there is a minimal effect of friction variation on oblique toppling. The friction cone controls oblique failure and not the slope face angle, hence a constant failure percentage regardless of the slope angle. Again, from the chart it is noted that as slope angle increases, direct toppling and basal plane for all sets of discontinuities also increased. A steady/noticeable rate of increase in failure due to basal toppling is noted as the slope angle increased from 65° to 85°. This sums up the observation made above in which it was explained that the extent of direct/basal toppling is directly related to the slope angle and the creation of rectangular columns as the slope angle nears vertical.

4.1.4 Flexural Toppling

A considerable risk of failure due to flexural toppling was also recorded in the results. Like any other failure mechanism to be achieved as explained above, certain conditions have to be satisfied. First condition for flexural toppling to happen a set of discontinuity should exist that dips into the slope and a formation of rectangular thin section with the slope face angle. The dip direction should also lie within the lateral limits of the slope dip direction (±20°). Unlike direct toppling, flexural toppling does not require a basal plane to act as a release plane. Considering the condition $\psi \geq 90 + \phi - \beta$ where ψ represents the slope face angle, φ represents the friction angle and β for dip of the interlayer discontinuity; it is observed that all the discontinuity sets satisfy this condition and specifically set 3m is more prone to failure by flexural toppling than the other discontinuity sets.

Results of kinematic analysis show that set 3m of discontinuity, which dips into the slope experiences a highest change of percentage in terms of risk of failure (see appendices 9 to 11). The slope face angle becomes the major contributor to the risk of flexural failure. A set of nearly vertical columns (rectangular thin sections) form during flexural failure, formed by either of the two steeply dipping sets (1m or 2m) and the slope face dip, which fall by plunging. These rectangular thin sections/columns are formed in conjunction with the discontinuity that dips into the slope.

It is observed that the risk of flexural failure increases as the slope face angle increases. No significant threat of failure is observed in the other two sets. This explains the observation made in the subsequent paragraph. At a slope angle of 45°, the failure is minimal. A moderate risk of failure in set 3m is observed when the slope face angle is set to the mean angle (65°). This is because there is a considerable formation of blocks to satisfy toppling as the slope face angle slowly approaches vertical. Set 2m has some poles that dips into the slope, however they are out of the limit range (lateral limits) of the slope dip direction for them to contribute failure by flexural toppling.

At a slope face angle of 85°, the risk of flexural toppling increases to 42%. At this slope angle, a significant failure risk is observed in set 3m. This makes sense due to two main reasons; as the slope angle increases more poles of set 3m are day lighted and covered by flexural toppling failure envelope. Secondly, the steep slope face results in a more conducive environment/condition for thin rectangular and vertical columns to form in relation to set 1m or 2m. A plunging effect therefore controlled by set 3m becomes effective.

Sensitivity analysis results do not vary with the observation made above. Figure 6 in the results section indicates there is a nearly positive linear relationship between the slope face angle and the percentage of failure. Slope dip direction indicates a negative linear risk of failure as the slope angle is brought to the mean dip direction. An increase in

failure percentage is observed a little after the mean dip direction angle and then it starts to fall again. This is due to the varying amount of poles enveloped by the flexural failure envelope as the slope dip direction varies. A wider lateral limit means set 3m would be widely covered by flexural toppling failure envelope. Hence, a positive linear increase in risk of failure as the lateral limit increases from 10° to 30°.

Slope dip direction and lateral limits in this case act as controlling factors of how much of set 3m should be covered by the failure envelope. Moving in either direction would determine the percentage of poles covered in set 3m to constitute flexural failure.

Friction angle portrays a linear relationship to the critical percentage. As observed from the chart, an increase in friction angle results in a reduction of the critical percentage of failure. However, the effect of varying friction is minimal and not highly pronounced.

4.2 Rockfall Analysis

Rockfall is highly dependent on the failure mechanisms described above. Without plane, wedge or any other failure little or no rockfall would be experienced on a slope. From the geotechnical analysis, it is observed that critical flexural toppling and wedge failure dominate on the slope as the major failure mechanisms. This is further attributed to the steepness of the slope. Basically, any rock falling at a height of 60m would cause damage as it falls. Due to the two critical failure mechanisms described above, it is certain that rockfall would follow on the slope.

From the cross-sections used for rockfall it is clear that as one goes up the slope above the road section, the slope becomes steeper. Normally, it is the haulage section (road) which is used by staff and equipment to move from one section of the slope to the other. Hence, the steep slope coupled with use of the road section creates a significant hazard in terms of rockfall on the road section. The section going down the slope after the road possess another significant threat in terms of hazard associated with rockfall. This is because the bottom of the slope would still be productive and mined. It therefore meant staff and/or equipment would be within that bottom section of the slope during mining operations.

4.2.1 Left section of the slope

As seen from the results in Figure 7, a single rock released from the top most part of the slope is able to go down to the bottom of the slope without stopping. The same happens with rocks seeded in the middle section and bottom part of the slope. The trajectory taken by a single rock shows that it first hits the haul road before proceeding to the bottom of the slope. A more severe impact on the road section is seen when 50 rocks are seeded on the slope section. From the section dimensions, the rock seeded at the top most of the slope falls a distance close to 40m before hitting the road section and proceeding down the slope.

Due to the height and steepness of the slope, the rocks possess the highest kinetic energy before hitting the road section. It is therefore a very high safety risk around the road section with some rocks possessing up to 200 kJ of energy. The energy dwindles down as the rock proceeds down the slope to the bottom. Due to less steepness of the section as well as short distance.

4.2.2 Centre section of the slope

The centre cross-section of the slope is the steepest amongst the three. From the simulation results in Figure 8 it is observed that a rock has to fall a distance of 50m or more to reach the road section only. Regardless of the weight of the rock falling at a

particular time, the destructive power carried by this rock could be severe. Most of the rocks falling above the road on this cross section are caught by the berm at the edge of the road. Therefore, two problems could be associated with rocks falling on this slope section, the first is the destructive energy on the equipment and/or people moving around the road section, and secondly piling of the rocks as they fall on the road section.

Similar hazard associated with left section is also observed on this cross section in terms of kinetic energy. Most of the rocks from the steepest top part of the slope end up on the road section and can therefore cause a great damage to both property and human beings on the mine.

4.2.3 Right section of the slope

This is the least steep section of the whole slope. The slope angle fluctuates within the mean angle (65°). In the results, Figure 9 shows that most of the rocks seeded on the top most section above the haul road do not land on the road. However, the rocks seeded on the middle section do land on the road but the energy carried with them is lower than what could have been carried by the rocks seeded on the highest point of the slope. Rocks falling from the highest point of the slope fall directly to the bottom section of the slope with a few bouncing on the slope.

Although falling rocks from the top most part do not go through the road, the ones that reach the road section still possess severe hazard. Therefore, the section possesses the same threat as the other cross sections of the slope. This is also evidenced by the distribution of kinetic energy amongst the rocks falling through the road section. The rocks carry similar kinetic energy like the other two sections.

5. DISCUSSION AND CONCLUSION

Remote mapping has been proved to be more significant and convenient in as far as rock slope characterization is concerned. Its flexibility and easy to analyse and interpret point cloud data makes it a very efficient method for geotechnical analysis. It is by far the most reliable method specifically for slopes where physical access (like the slope under observation here) is restricted. It is also one of the most effective ways to obtain geotechnical data especially in slopes where safety could be of greater concern.

Furthermore, without the use of stereographic projection software (Dips) one is able to determine indicative results from the use of Split FX software. The possibility of automatically plotting data on a stereo-net during patching and tracing in point cloud allows the user to make preliminary observation of the type of failure mechanisms to be anticipated. This comes handy in cases where swift decisions have to be made on the possible failure mechanisms on a slope in the absence of the extensive kinematic analysis from Dips software.

Despite requiring special skills to both use the laser-scanning machine and setting up of the whole system, the time taken to obtain extensive data over a wide range of space is highly reduced. In addition, the data obtained is of high clarity (depending on the type of scanning machine used) and an accurate representation of the slope. This is a revolutionary system in geotechnical engineering and is most effective and convenient in terms of rock slope mapping.

A thorough look at the results for both stereographic projection (Dips) and rockfall simulation indicates that the quarry slope possesses a serious threat in terms of failure. As observed from the results, the major failure mechanisms associated with the slope are wedge and flexural toppling. However, regardless of low percentage/likelihood in failure

for the other failure mechanisms, the slope can still fail courtesy of them. This comes from the fact that the actual/exact location of failure, the severity and the time it might be cannot be ascertained through kinematic analysis. Nevertheless, a high percentage of failure as indicated by kinematic gives enough evidence of critical and likelihood failure by the given mechanisms, in this case flexural toppling and wedge failure.

Further analysis using Swedge shows a low factor of safety in terms of stability against sliding. This low factor of safety was attributed to the steepness of the slope. However, further addition of external forces such as groundwater effect on the releasing joint surfaces could reduce further the stability of the wedge formation. Therefore, this shows how severe and risky the slope is in terms of discontinuity related failure.

In addition, the steepness of the slope (especially the top most part after the haul road) makes the rock slope very prone to rockfall. The major hazard location for rockfall is associated with road section. The fact that human beings and equipment/property ideally use the road section for mining operations increases the hazard the road possess in terms of accidents/damage due to rockfall. This in turn increases the risk and threat to safety of operations for the quarry mine. In summary, discontinuity related failure (wedge and flexural toppling) explained above coupled with the steepness of the slope provides a conducive environment for rockfall.

As mentioned above, the failure mechanisms would result in rockfall. The geometry of the slope shows that significant rock fall would emanate from the top most section of the slope (above the road). This would result in reduced or no production on the quarry mine. Hence the need for remedial measures to control rockfall and maintain production. Due to the steepness of the slope section above the road, no more production can take place because of safety reasons. However, the bottom section of the slope including the talus can still be productive.

The main idea is to control rocks falling from the top section and prevent them from reaching the bottom part of the slope where production would still take place. This can therefore be done by putting in place a barrier along the road from one end to the other. The barrier would block rocks falling from the top section of the slope. The road section would therefore act as a collection mechanism for the falling rocks (collecting basin). Figures 10 to 26 in appendixes have illustrated three cross-sections of the slope and location of the proposed barrier on the road. It also shows ideally how the barriers would block the rocks as they fall.

It has to be emphasized that the results illustrated in this research only relate to discontinuity related failure. Further research therefore needs to be done on stress related failure. It can also be observed that the influence of groundwater on the stability of the slope has not been addressed in this paper. This is another area that would also need further research to look at the effects of groundwater on the overall stability of the slope.

CONFLICT OF INTEREST

The authors confirm that there is no conflict of interests associated with this publication and there is no financial fund for this work that can affect the research outcomes.

REFERENCES

[1] Salmon J. (June 2017) Mineral Planning: Extension removes barriers, Environmental Data Services (ENDS).

Available: http://www.mineralandwasteplanning.co.uk/extension-removes-old-barriers/building-stone/article/1429659.

[2] Coggan J.S., Wetherelt A., Gwynn X.P. and Flynn Z.N. (2007) Comparison of hand mapping with remote data capture systems for effective rock mass characterization. *11th Congress of the International Society for Rock Mechanics*, Lisbon, Portugal, p. 1-45.

[3] Gwynn X.P. (2008) "Assessment of Remote Data Capture Systems for the Characterisation of Rock Fracture Networks within Slopes," *Ph.D. dissertation*, Camborne School of Mines, School of Geography Archaeology and Earth Resources, University of Exeter.

[4] Slama I. (1980) Manual of photogrammetry. 4th edition. American Society of Photogrammetry, Virginia, US.

[5] Mcglone C. J. Manual of photogrammetry. 5th edition, American Society for Photogrammetry and Remote Sensing, Maryland, US. 2004.

[6] Feng Q., Sjogren P., Stephansson O. and Jing L. Measuring fracture orientation at exposed rock faces by using a non-reflector total station. *Engineering Geology*, 2001; 59; 133-146.

[7] Wani S. B. Analytical Study on the Influence of Rib Beams on the Stability of RCC Dome Structures. *International Journal of Innovative Technology and Interdisciplinary Sciences*, 2020; 3(3), 480-489.

[8] Hoek E. T. (2016) Rock engineering course notes. Chapter 9: Analysis of rockfall hazards. http://www.rocscience.com/roc/Hoek/Hoeknotes2000.htmS

[9] Pine R. J., Lay S., Randall M. M., and Trueman R. (1992) Rock Engineering Developments at South Crofty Mine.

[10] Afzulpurkar N. New Approach for a Fault Detect Model-Based Controller. *International Journal of Innovative Technology and Interdisciplinary Sciences*, 2019; 2(2); 160-172.

.

APPENDIXES

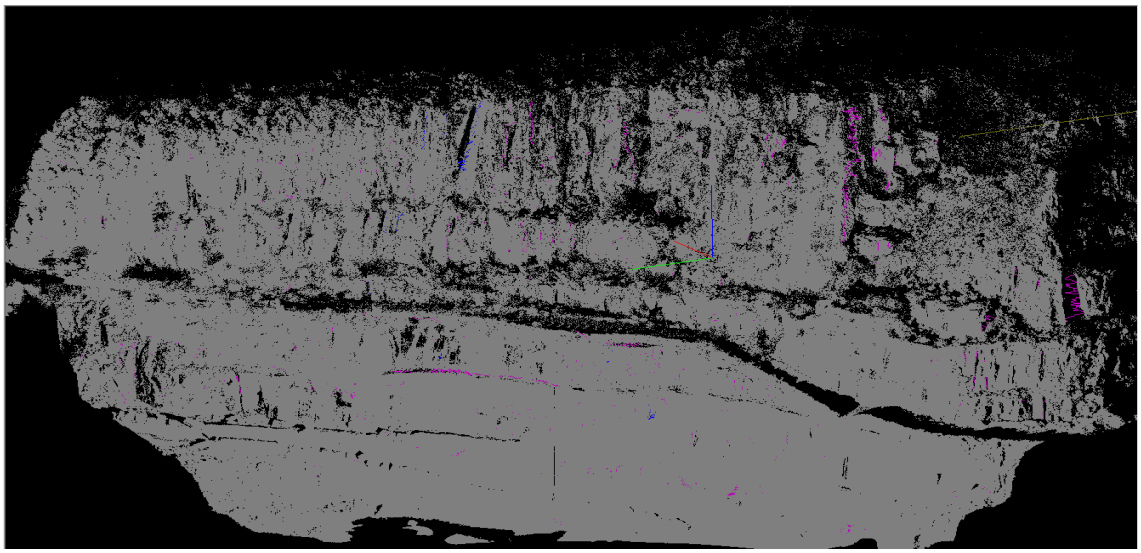

Figure 10. Point cloud data of the slope section under consideration.

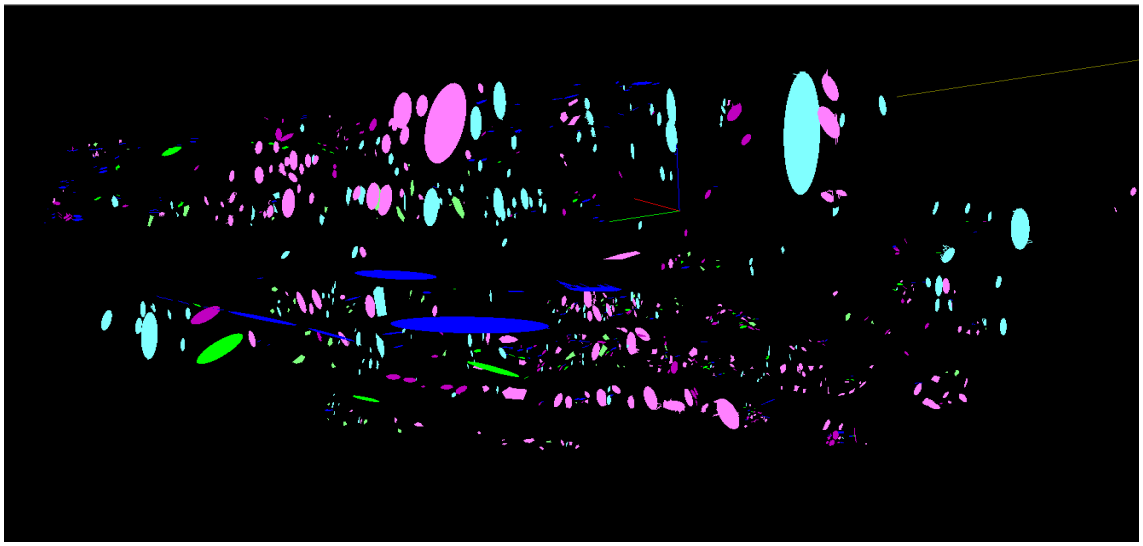

Figure 11. Point cloud data in Split FX software showing patches and traces obtained during mapping.

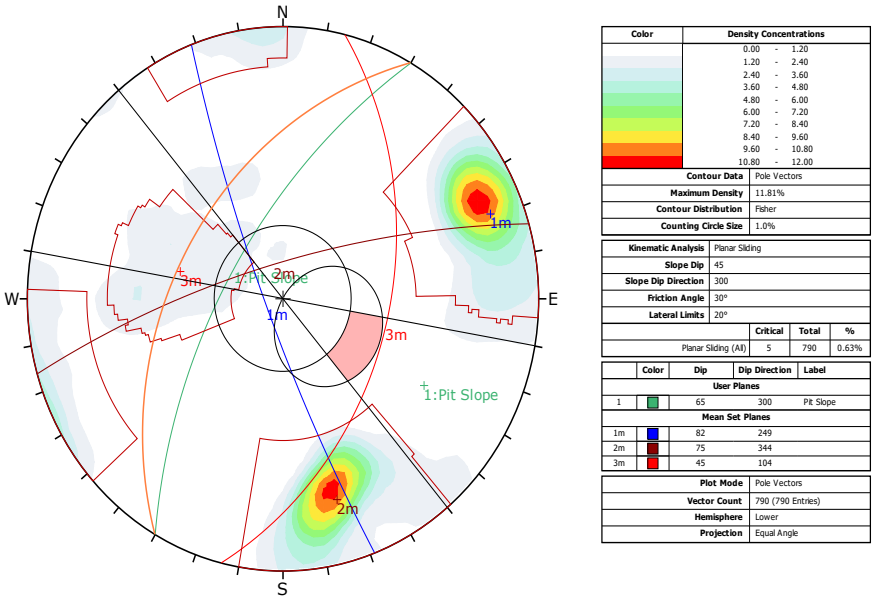

Figure 12. Kinematic analysis of plane failure with minimum slope angle (45°)

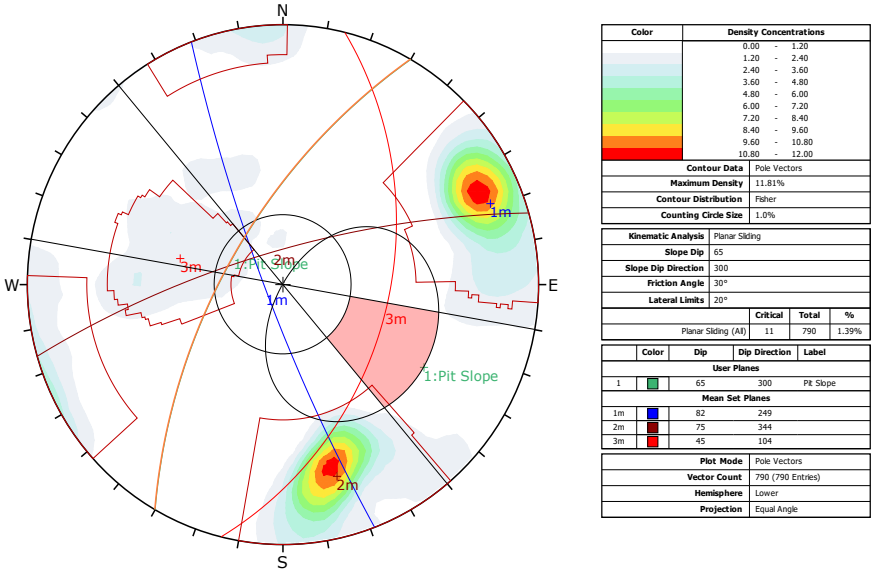

Figure 13. Kinematic analysis of plane failure with mean slope angle (65°)

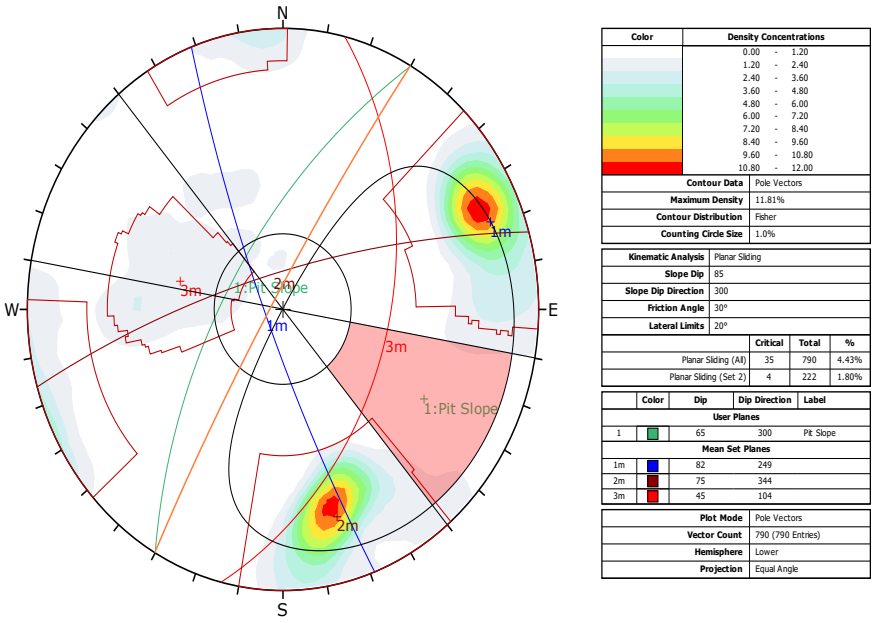

Figure 14. Kinematic analysis of plane failure with maximum slope angle (85°)

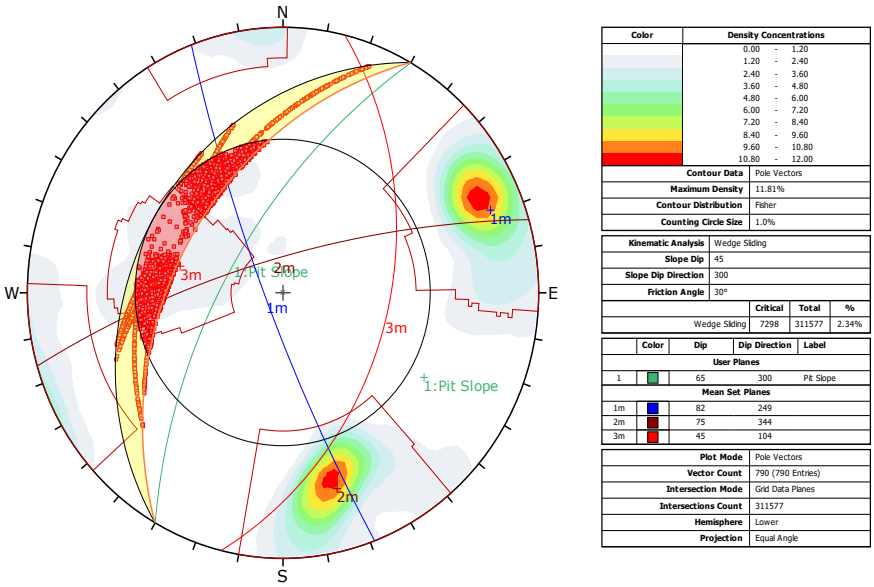

Figure 15. Kinematic analysis of wedge failure with minimum slope angle (45°)

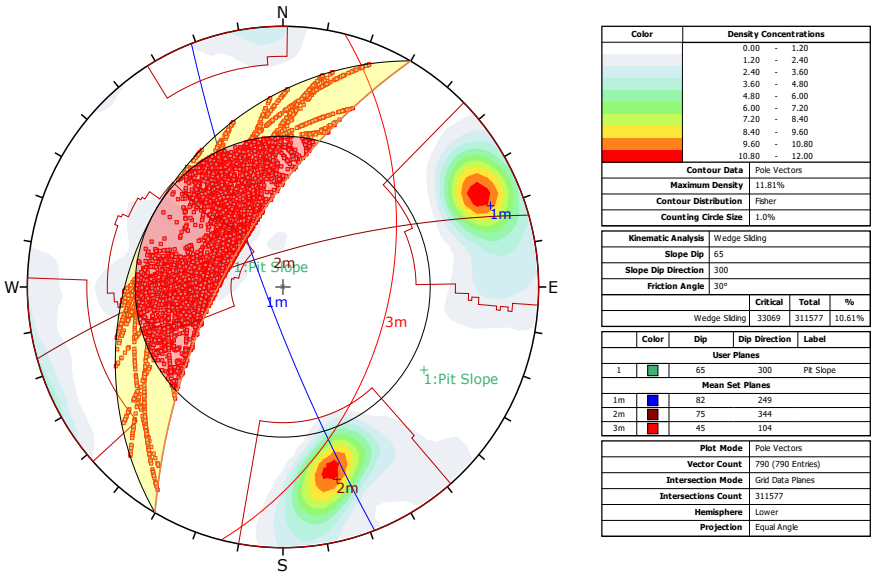

Color	Density Concentrations
	0.00 - 1.20
	1.20 - 2.40
	2.40 - 3.60
	3.60 - 4.80
	4.80 - 6.00
	6.00 - 7.20
	7.20 - 8.40
	8.40 - 9.60
	9.60 - 10.80
	10.80 - 12.00

Contour Data	Pole Vectors
Maximum Density	11.81%
Contour Distribution	Fisher
Counting Circle Size	1.0%

Kinematic Analysis	Wedge Sliding
Slope Dip	65
Slope Dip Direction	300
Friction Angle	30°

	Critical	Total	%
Wedge Sliding	33069	311577	10.61%

	Color	Dip	Dip Direction	Label
User Planes				
1		65	300	Pit Slope
Mean Set Planes				
1m		82	249	
2m		75	344	
3m		45	104	

Plot Mode	Pole Vectors
Vector Count	790 (790 Entries)
Intersection Mode	Grid Data Planes
Intersections Count	311577
Hemisphere	Lower
Projection	Equal Angle

Figure 16. Kinematic analysis of wedge failure with mean slope angle (65°)

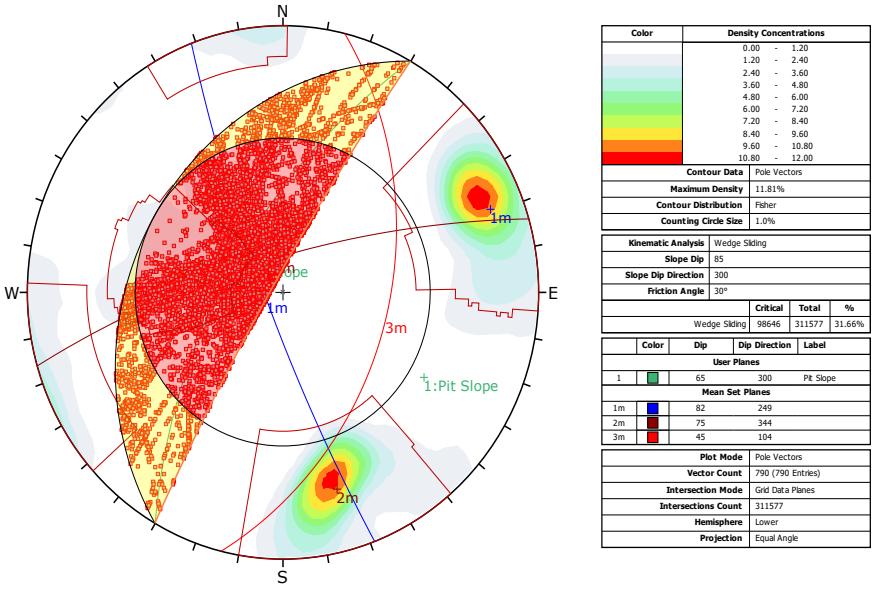

Color	Density Concentrations
	0.00 - 1.20
	1.20 - 2.40
	2.40 - 3.60
	3.60 - 4.80
	4.80 - 6.00
	6.00 - 7.20
	7.20 - 8.40
	8.40 - 9.60
	9.60 - 10.80
	10.80 - 12.00

Contour Data	Pole Vectors
Maximum Density	11.81%
Contour Distribution	Fisher
Counting Circle Size	1.0%

Kinematic Analysis	Wedge Sliding
Slope Dip	85
Slope Dip Direction	300
Friction Angle	30°

	Critical	Total	%
Wedge Sliding	98646	311577	31.66%

	Color	Dip	Dip Direction	Label
User Planes				
1		65	300	Pit Slope
Mean Set Planes				
1m		82	249	
2m		75	344	
3m		45	104	

Plot Mode	Pole Vectors
Vector Count	790 (790 Entries)
Intersection Mode	Grid Data Planes
Intersections Count	311577
Hemisphere	Lower
Projection	Equal Angle

Figure 17. Kinematic analysis of wedge failure with maximum slope angle (85°)

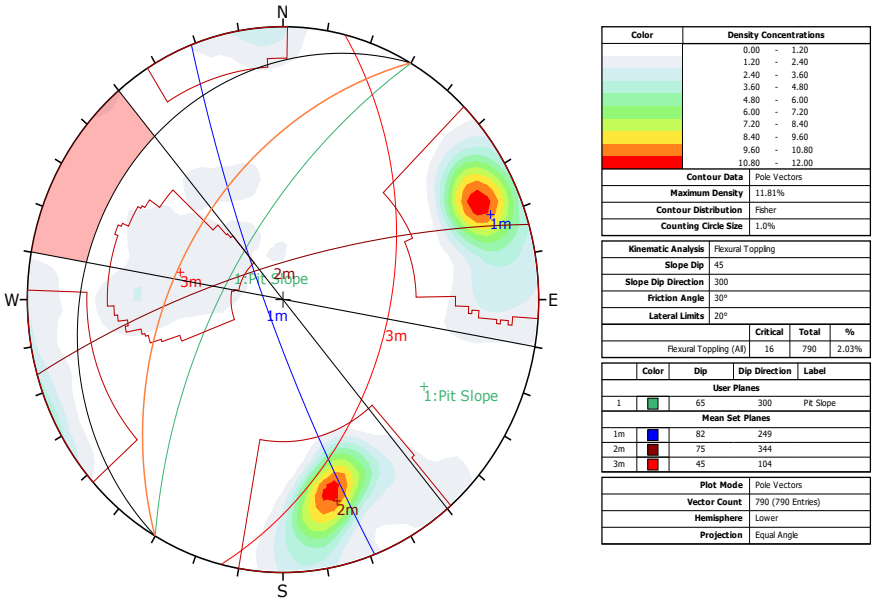

Figure 18. Kinematic analysis of flexural toppling with minimum slope angle (45°)

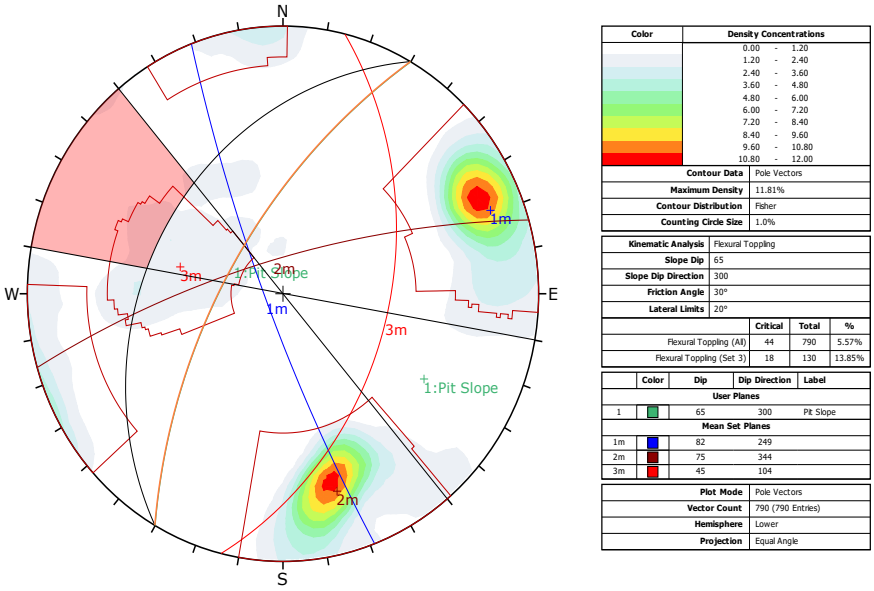

Figure 19. Kinematic analysis of flexural toppling with mean slope angle (65°)

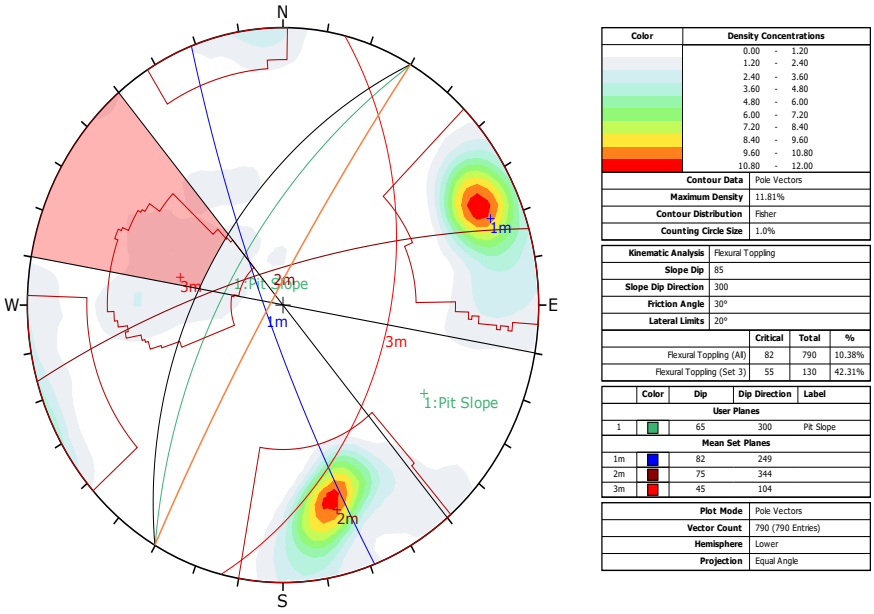

Color	Density Concentrations
	0.00 - 1.20
	1.20 - 2.40
	2.40 - 3.60
	3.60 - 4.80
	4.80 - 6.00
	6.00 - 7.20
	7.20 - 8.40
	8.40 - 9.60
	9.60 - 10.80
	10.80 - 12.00
Contour Data	Pole Vectors
Maximum Density	11.81%
Contour Distribution	Fisher
Counting Circle Size	1.0%

Kinematic Analysis	Flexural Toppling
Slope Dip	85
Slope Dip Direction	300
Friction Angle	30°
Lateral Limits	20°

	Critical	Total	%
Flexural Toppling (All)	82	790	10.38%
Flexural Toppling (Set 3)	55	130	42.31%

	Color	Dip	Dip Direction	Label
User Planes				
1		65	300	Pit Slope
Mean Set Planes				
1m		82	249	
2m		75	344	
3m		45	104	

Plot Mode	Pole Vectors
Vector Count	790 (790 Entries)
Hemisphere	Lower
Projection	Equal Angle

Figure 20. Kinematic analysis of flexural toppling with maximum slope angle (85°)

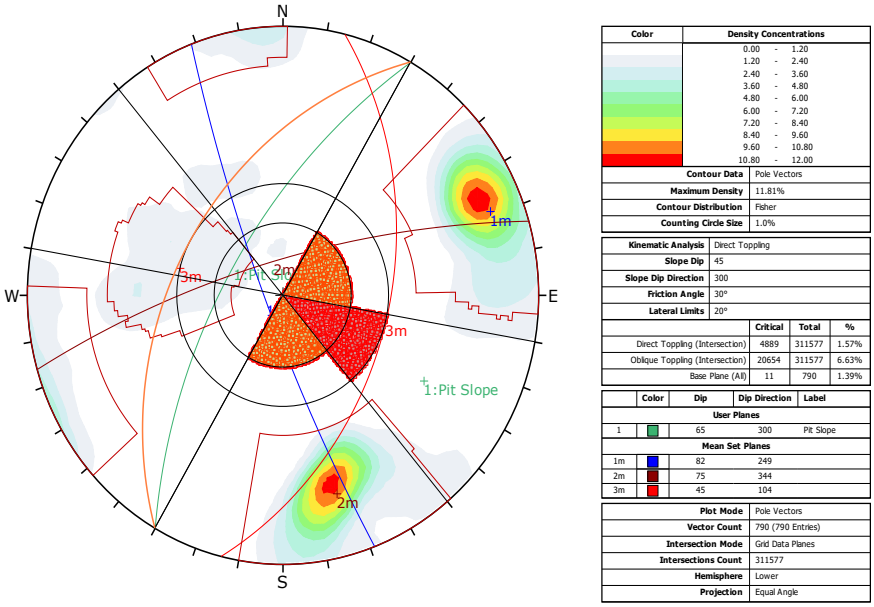

Color	Density Concentrations
	0.00 - 1.20
	1.20 - 2.40
	2.40 - 3.60
	3.60 - 4.80
	4.80 - 6.00
	6.00 - 7.20
	7.20 - 8.40
	8.40 - 9.60
	9.60 - 10.80
	10.80 - 12.00
Contour Data	Pole Vectors
Maximum Density	11.81%
Contour Distribution	Fisher
Counting Circle Size	1.0%

Kinematic Analysis	Direct Toppling
Slope Dip	45
Slope Dip Direction	300
Friction Angle	30°
Lateral Limits	20°

	Critical	Total	%
Direct Toppling (Intersection)	4889	311577	1.57%
Oblique Toppling (Intersection)	20654	311577	6.63%
Base Plane (All)	11	790	1.39%

	Color	Dip	Dip Direction	Label
User Planes				
1		65	300	Pit Slope
Mean Set Planes				
1m		82	249	
2m		75	344	
3m		45	104	

Plot Mode	Pole Vectors
Vector Count	790 (790 Entries)
Intersection Mode	Grid Data Planes
Intersections Count	311577
Hemisphere	Lower
Projection	Equal Angle

Figure 21. Kinematic analysis of direct and oblique toppling with minimum slope angle (45°)

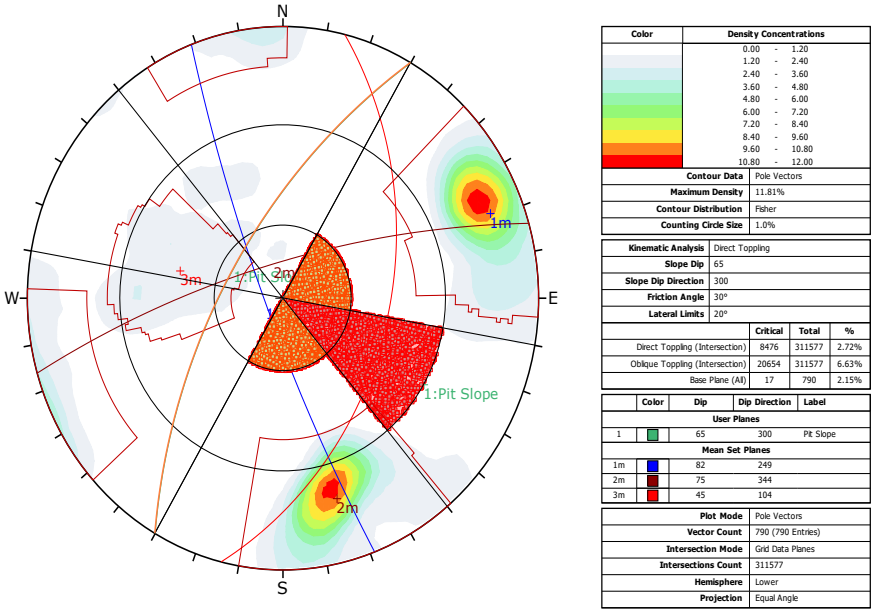

Color	Density Concentrations
	0.00 - 1.20
	1.20 - 2.40
	2.40 - 3.60
	3.60 - 4.80
	4.80 - 6.00
	6.00 - 7.20
	7.20 - 8.40
	8.40 - 9.60
	9.60 - 10.80
	10.80 - 12.00

Contour Data	Pole Vectors
Maximum Density	11.81%
Contour Distribution	Fisher
Counting Circle Size	1.0%

Kinematic Analysis	Direct Toppling
Slope Dip	65
Slope Dip Direction	300
Friction Angle	30°
Lateral Limits	20°

	Critical	Total	%
Direct Toppling (Intersection)	8476	311577	2.72%
Oblique Toppling (Intersection)	20654	311577	6.63%
Base Plane (All)	17	790	2.15%

	Color	Dip	Dip Direction	Label
User Planes				
1		65	300	Pit Slope
Mean Set Planes				
1m		82	249	
2m		75	344	
3m		45	104	

Plot Mode	Pole Vectors
Vector Count	790 (790 Entries)
Intersection Mode	Grid Data Planes
Intersections Count	311577
Hemisphere	Lower
Projection	Equal Angle

Figure 22. Kinematic analysis of direct and oblique toppling with mean slope angle (65°)

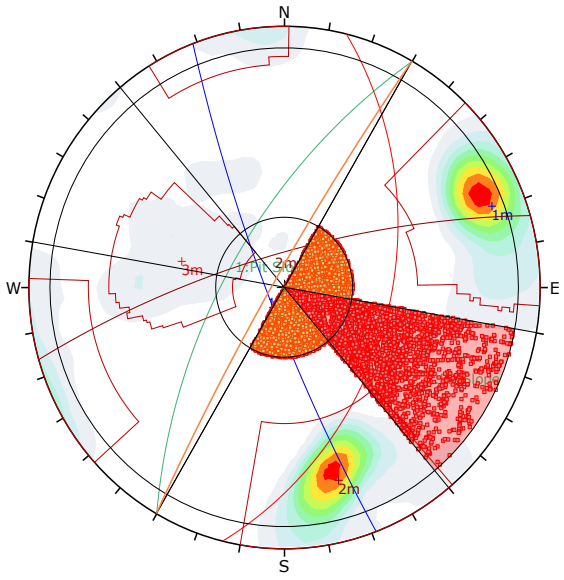

Color	Density Concentrations
	0.00 - 1.20
	1.20 - 2.40
	2.40 - 3.60
	3.60 - 4.80
	4.80 - 6.00
	6.00 - 7.20
	7.20 - 8.40
	8.40 - 9.60
	9.60 - 10.80
	10.80 - 12.00

Contour Data	Pole Vectors
Maximum Density	11.81%
Contour Distribution	Fisher
Counting Circle Size	1.0%

Kinematic Analysis	Direct Toppling
Slope Dip	85
Slope Dip Direction	300
Friction Angle	30°
Lateral Limits	20°

	Critical	Total	%
Direct Toppling (Intersection)	9925	311577	3.19%
Oblique Toppling (Intersection)	20654	311577	6.63%
Base Plane (All)	42	790	5.32%
Base Plane (Set 2)	4	222	1.80%

	Color	Dip	Dip Direction	Label
User Planes				
1		65	300	Pit Slope
Mean Set Planes				
1m		82	249	
2m		75	344	
3m		45	104	

Plot Mode	Pole Vectors
Vector Count	790 (790 Entries)
Intersection Mode	Grid Data Planes
Intersections Count	311577
Hemisphere	Lower
Projection	Equal Angle

Figure 23. Kinematic analysis of direct and oblique toppling with maximum slope angle (85°)

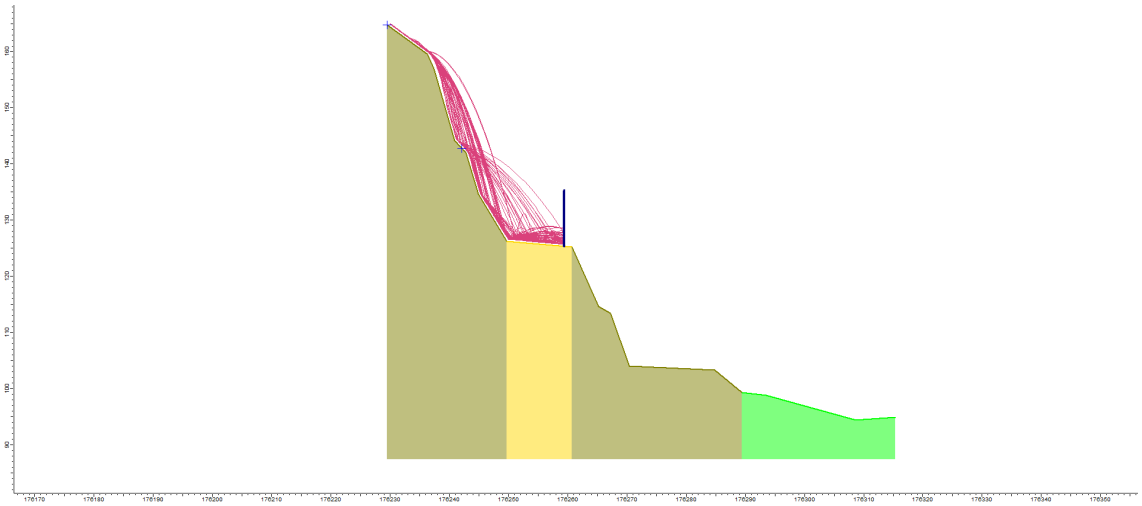

Figure 24. Left cross-section of the slope showing suggested location of the barrier and how it would control/block rocks.

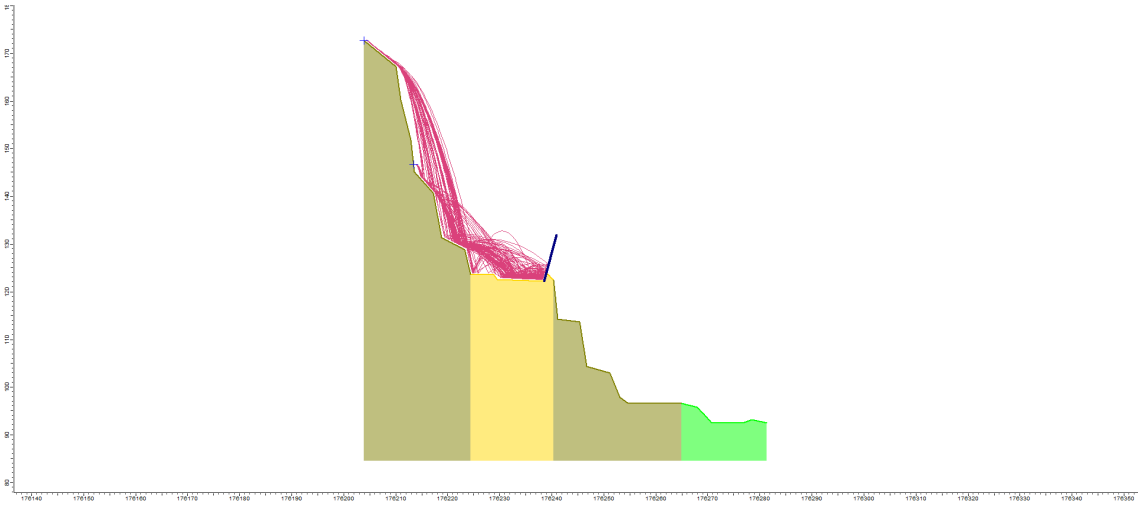

Figure 25. Centre cross-section of the slope showing suggested location of the barrier and how it would control/block rocks

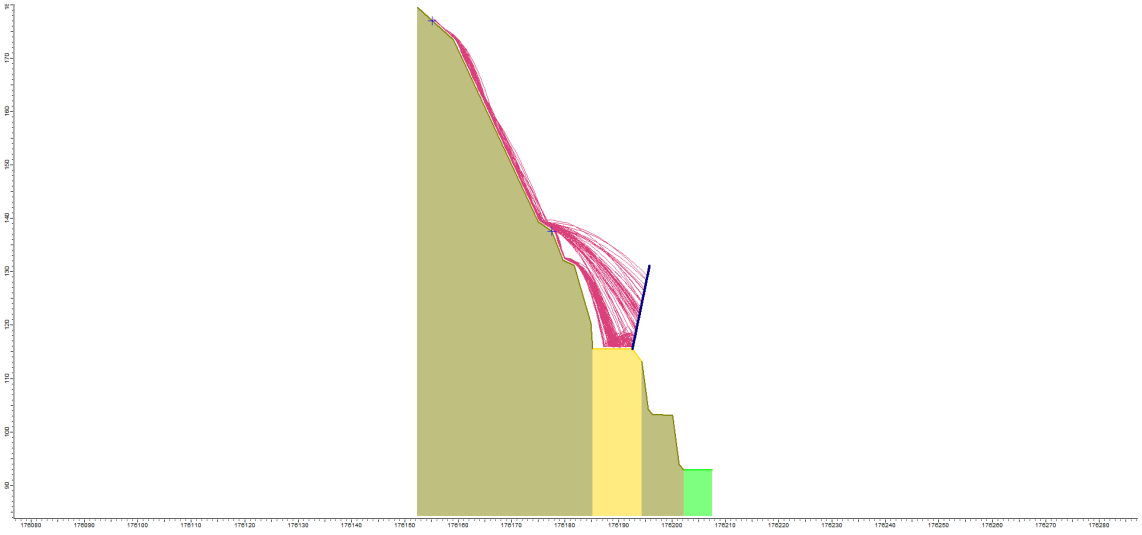

Figure 26. Right cross-section of the slope showing suggested location of the barrier and how it would control/block rocks